DRAFT VERSION FEBRUARY 2, 2026
Typeset using LaTeX **preprint** style in AASTeX631

Memo 4: UHF Phased Array Antenna and Beamformer Preliminary Design Study (Draft v1.0)

REBECCA HAYMORE,[1] DANIEL KEMP,[1] RYAN LARSEN,[1] CALEB EDMUNDS,[1] DAVID R. DEBOER,[2,3] AND KARL F. WARNICK[1]

[1]*ECE Dept., Brigham Young University, Provo, Utah, USA, warnick@byu.edu*
[2]*Sub-department of Astrophysics, University of Oxford, Oxford, OX1-3RH, UK*
[3]*Radio Astronomy Laboratory, University of California, Berkeley, CA, 94720 USA*

1. INTRODUCTION

The Lunar Farside Technosignatures and Transients Telescope (LFT3) will search the lunar sky for radio emissions for known and unknown sources and create an unprecedented historical record of radio observations on the moon (1). The lunar farside offers a unique environment to measure radiation from the Universe with essentially zero radio frequency interference. The planned LFT3 sensor package will include single antennas for 1-50 MHz and 60-110 MHz, a wideband antenna array occupying the bulk of the lander top surface operating in the band 300-900 MHz (UHF-Lo), and a secondary higher frequency interleaved array in the band 900-2700 MHz (UHF-Hi). The UHF arrays will form multiple beams on the lunar sky. The beamformer and signal acquisition system designs are constrained by the requirement that LFT3 operate continuously through lunar day and night. To avoid excess weight and launch cost for the batteries, low power operation is required.

Major components of the UHF-Lo receiver include a wideband antenna array, front end low noise amplifiers, beamformer, downconverters, and digital signal processing. The array element design for the UHF-Lo receiver is a modified version of the dual-polarized Vivaldi feed used for the HERA instrument (2). To avoid the high power consumption of a digital beamformer, an analog beamformer design has been selected.

The low-power, wideband analog UHF-Lo beamformer is the major new technology development effort for the array. The brute-force approach to the design of an analog beamformer is power splitters after each array element to distribute received signals to a beamforming network for each beam. To reduce the size and complexity of the beamformer, time delays are distributed across a two-dimensional grid in a Blass matrix (3; 4). We have developed a modified Blass matrix approach that trades an increase in complexity for improved accuracy of time delays over a wide bandwidth. The beam patterns realized by the analog beamformer are fixed at manufacture and no calibration is needed or possible. Other designs were considered including a Rotman lens on high dielectric constant substrate but likely not feasible due to the large required size. The selected design approach is a highly reliable, low-risk yet technologically innovative solution for the UHF-Lo receiver.

Signals from the midband array and other antennas on the lander will be downconverted to a 50 MHz bandwidth tuned in steps over the 300-900 MHz midband array operating frequency. A multichannel digitizer and FPGA-based spectrometer will be used to compute frequency spectra for transmission to a lunar orbiter and downlinking to earth. The spectrometer will operate in full mode during lunar day and a reduced

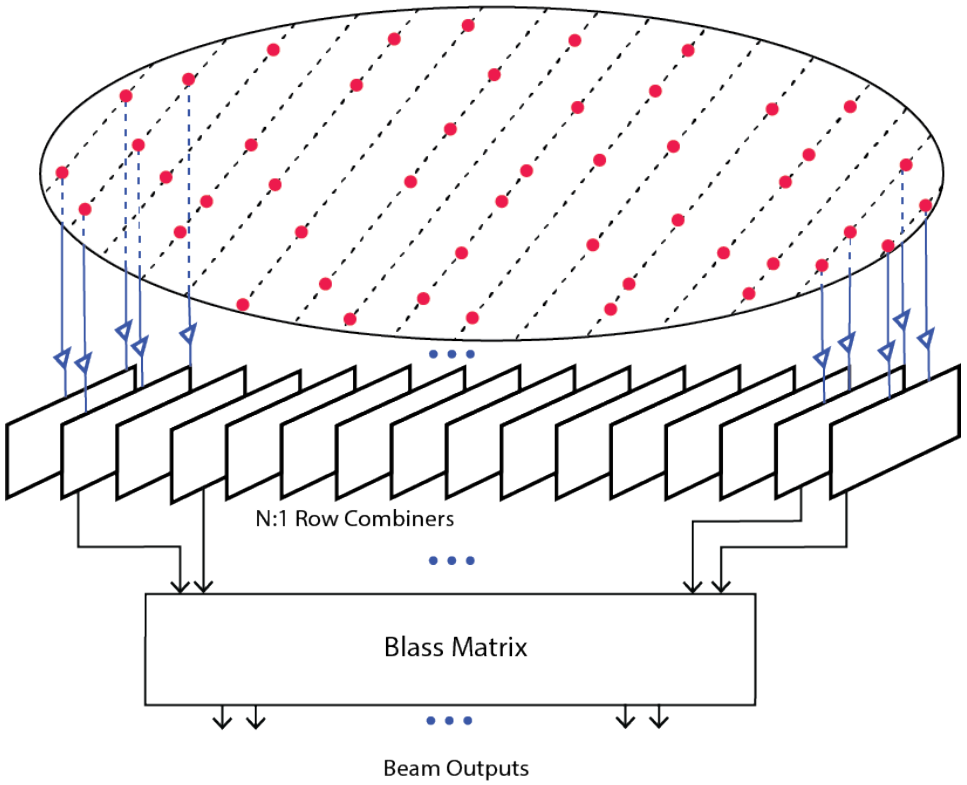

Figure 1. UHF-Lo array and beamformer diagram. Since the formed beams are spaced along a linear field of view and steered only in one axis, each row of the array requires only one combiner. The row signals are then fed to a modified Blass matrix beamformer to produce ten formed beams.

power mode during lunar night (5). Spectra will be computed for 50 MHz subbands with a high resolution (on the order of 1 kHz), specifically targeting technosignature searches.

In this memo, we provide design details for the UHF-Lo antenna array, beamforming network, and RF signal handling stages. Results are given for prototyped components of the UHF-Lo array including test results for the analog beamformer and measured antenna patterns. Design considerations and simulated results are also given for a Rotman lens beamformer under consideration for the LFT3 UHF-Hi array receiver. The next major step in the receiver development effort is fabrication of the full UHF-Lo beamformer and an engineering test hardware implementation of the full receiver system.

2. LFT3 UHF PHASED ARRAY RECEIVER SYSTEM DESIGN

The science requirements for the LFT3 mission in the UHF band require high sensitivity and a sufficiently large field of view to cover the lunar sky over time. Full time operation with limited battery capacity over lunar night dictate that the scientific payload function with a low power requirement. Accordingly, design goals for the UHF-Lo receiver include high sensitivity, a field of view that covers the full lunar sky over time, and a passive beamformer that requires no DC power.

Figure 1 shows a functional diagram of the UHF-Lo beamformer. The RF signal chain includes low noise amplifiers, power combiners, and a wideband, true time delay beamformer. The two-stage analog beamformer system combines signals from the array into beams steered along a linear field of view on the lunar sky.

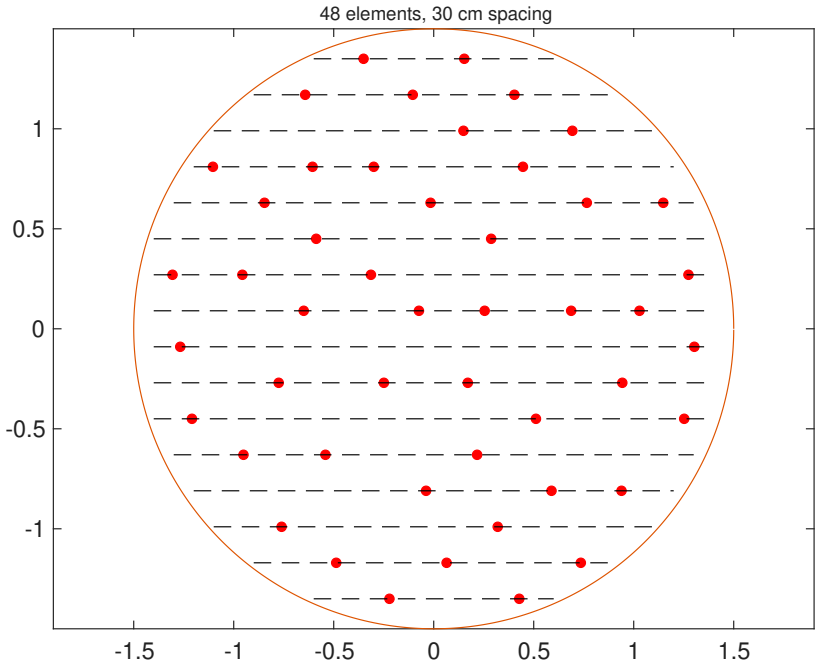

Figure 2. UHF-Lo array layout. To simplify the design of the analog beamformer, element locations are constrained to horizontal rows.

2.1. *UHF-Lo Array Geometry*

The UHF-Lo array (ULA) consists of 48 dual-polarized Vivaldi antenna elements with pseudorandom locations on a 3 m circular aperture. The UHF-Lo array element layout was numerically optimized to allow beams to be formed with high aperture efficiency and low sidelobes, maximize the distance between elements, and minimize the complexity of the analog beamformer. Formed beams are aligned along a fan pattern that rotates across the sky over the course of a lunar day.

To allow for element outputs along rows in the direction orthogonal to the fan beam field of view to be combined with as few as possible inputs to the second stage beamformer, elements in the array are aligned in 16 equally spaced horizontal rows as shown in Fig. 2. Element locations in the horizontal direction were selected to minimize sidelobes of the formed beams. Signals from elements in each row are summed using equal-phase power combiners as shown in Fig. 1. The first stage of the beamformer reduces the array to a uniform linear array in the vertical direction with elements spaced 18 cm apart. Each element in the ULA is a subarray comprised of the antennas in one row of the full array. The first stage element row combiners are followed by a second beamformer stage consisting of a 16 input, ten output analog beamformer for each polarization to form beams along a line on the lunar sky.

Formed beams along a linear fan pattern are designed to be spaced at half power levels at midband (600 MHz) as shown in Fig. 3. The beams are superimposed to illustrate the field of view at 600 MHz in Fig. 4. The UHF-Lo array field of view at frequencies across the bandwidth of the receiver is shown in Fig. 5. At lower frequencies, there is redundancy in the beams due to high overlap. At higher frequencies, the beams narrow and the beams overlap at a lower level, leading to undersampling of the field of view.

The sensitivity of the formed beams at the center of the UHF-Lo bandwidth is shown in Fig. 6. The noise model includes sky noise, cosmic background radiation, and receiver noise. The equivalent system noise temperature is 35 K. Depending on the orientation of the beams relative to the galaxy, the sky noise

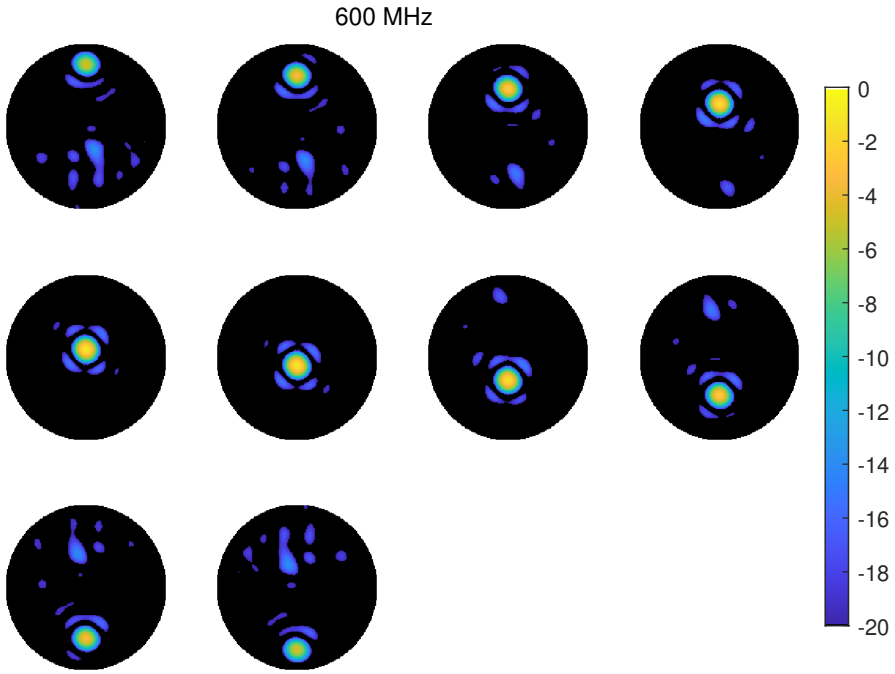

Figure 3. UHF-Lo formed beams at 600 MHz. The color scale shows aperture efficiency maps in dB for ten formed beams in dB relative to the 3 m diameter LFT3 lander top surface.

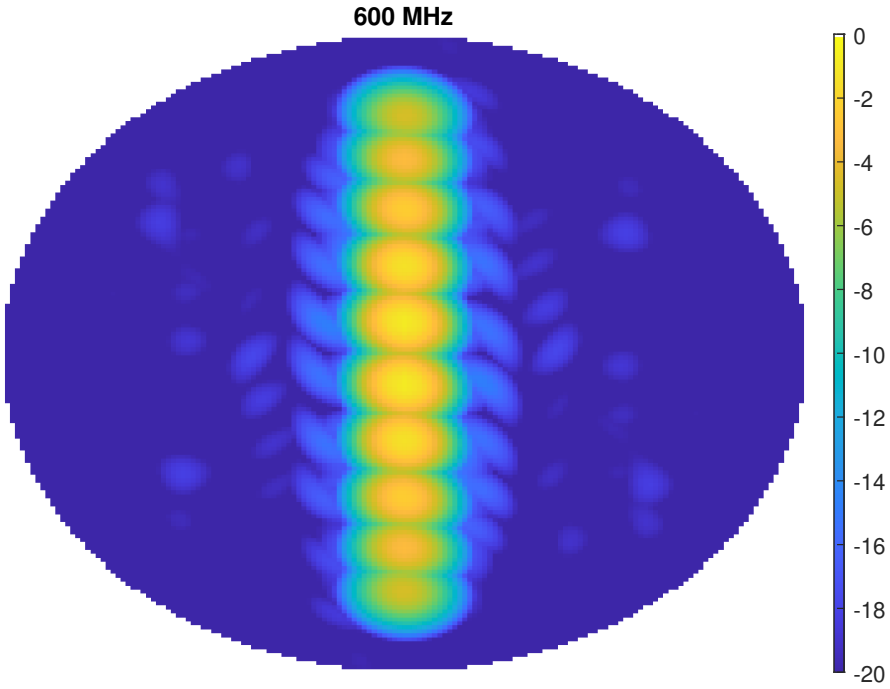

Figure 4. UHF-Lo field of view at 600 MHz with all formed beams combined.

contribution can be as high as several hundred Kelvin, so the value used in the beam sensitivity model represents a minimum over rotation of the lunar sky across the UHF-Lo field of view.

2.2. *Antenna Elements*

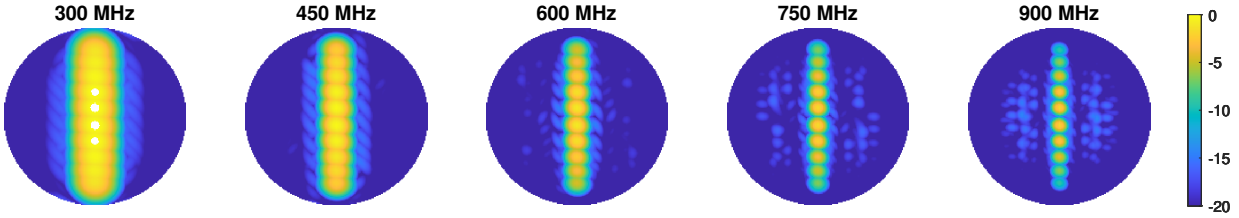

Figure 5. UHF-Lo field of view over the receiver bandwidth.

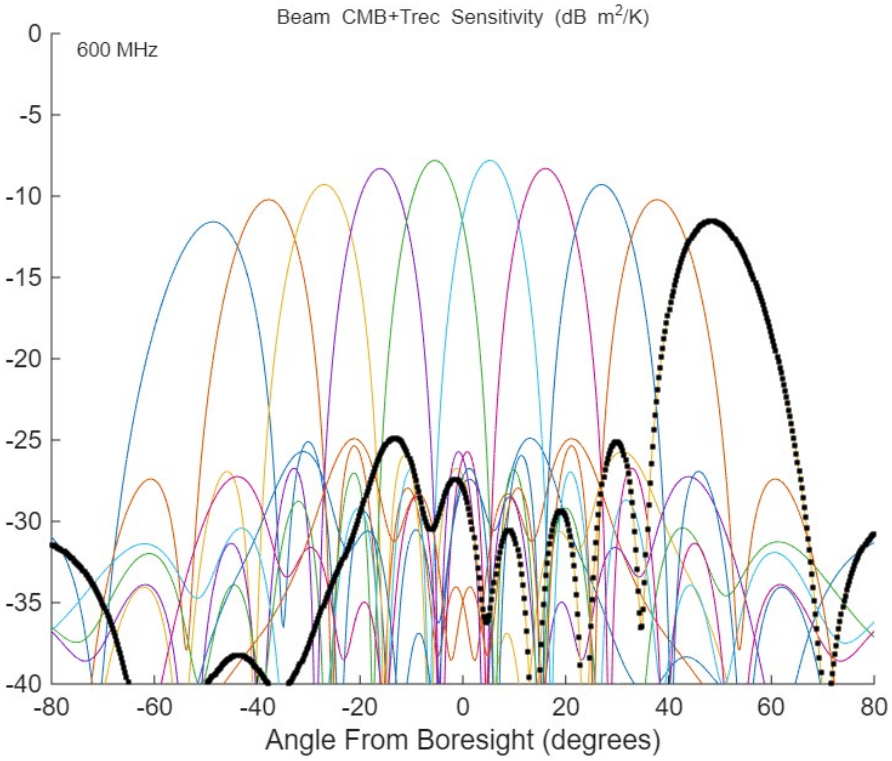

Figure 6. UHF-Lo beam sensitivity pattern cut at 600 MHz. The array geometry was optimized to minimize sidelobes of the formed beams to 10-15 dB below the main beam peak.

The Vivaldi antenna element design was primarily driven by the wideband frequency spectrum of the UHF-Lo array, 300-900 MHz. The geometrical shape of the antenna was parameterized for numerical optimization using exponentials and quarter ellipses. A finite element method forward model (HFSS, Ansys, Inc.) was used to tune the design to achieve return loss over the target bandwidth of 10 dB or better.

Once a suitable design was obtained, prototypes were fabricated and tested on PCB substrate. To facilitate fabrication on a PCB, the element was initially designed as an antipodal Vivaldi antenna. The initial fabricated antenna element on PCB was 18×27 cm. The antenna is shown in Fig. 7 and the modeled and measured input reflection coefficient in Fig. 8.

After testing of the PCB prototype, the antenna element was modified to be fabricated from an aluminum sheet. This required a change to the antenna feed structure. The aluminum element was prototyped by waterjet cutting. The aluminum prototypes dimensions were 21×29 cm. The antenna and input reflection coefficient are shown in Figs. 9 and 10.

2.3. *Low Noise Amplifiers (LNAs) and RF Subsystems*

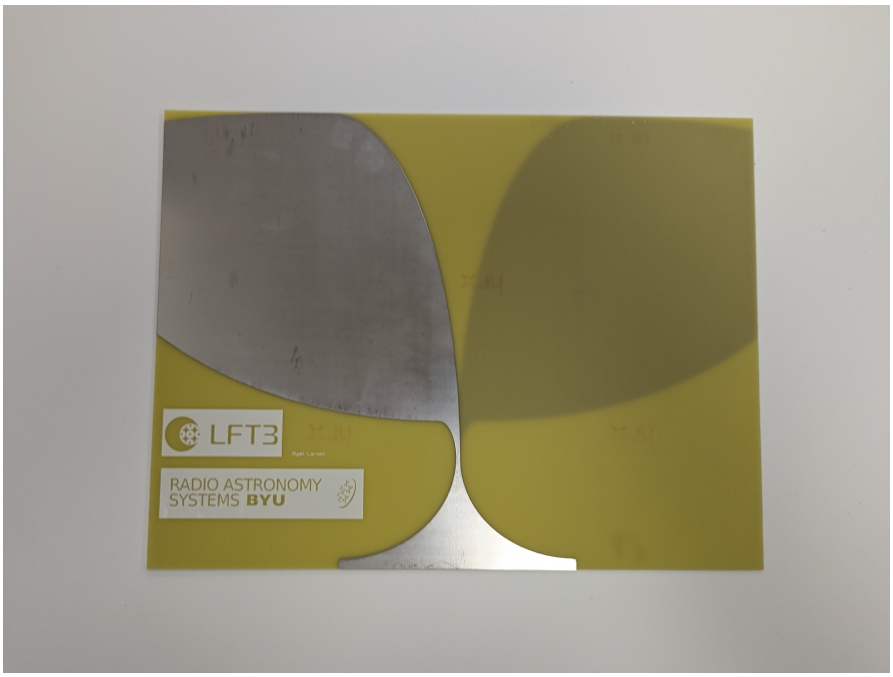

Figure 7. 300–900 MHz Vivaldi element PCB prototype.

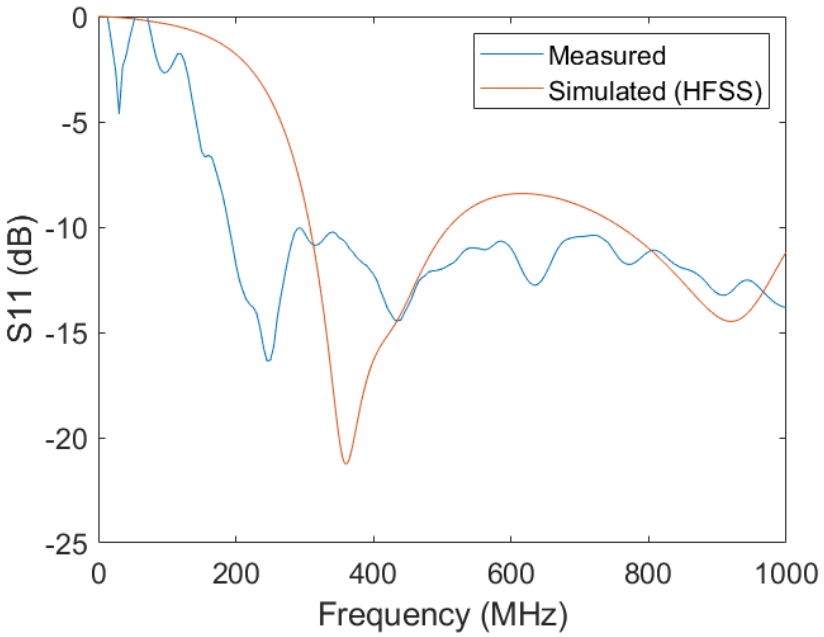

Figure 8. PCB fabricated Vivaldi prototype return loss.

Array elements are connected via transmission lines to a low noise amplifier (LNA) front end gain stage. To minimize heat transfer between the antenna elements and components inside the lander structure, the interconnects will use high thermal resistivity materials. Gain in the front end must be sufficient to ensure a low noise figure for the signal chain including losses in the beamforming network.

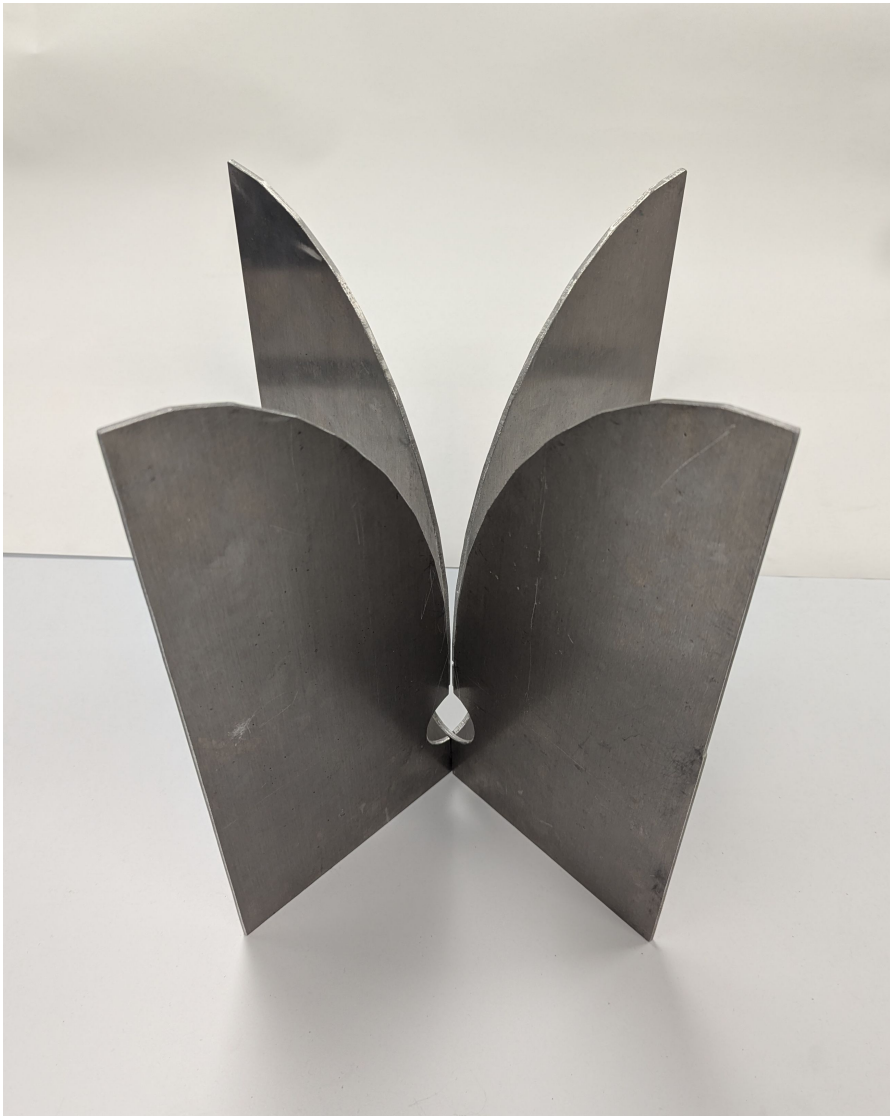

Figure 9. Dual-pol fabricated aluminum Vivaldi element prototype

To provide a prototype gain stage for the LFT3 antenna array, an LNA was designed and fabricated on printed circuit board. The board integrates a high-gain LNA stage to minimize noise contributions from later stages, followed by a filter that defines the operating bandwidth. The filter section consists of ganged high pass and low pass filters with passband 300–900 MHz. Measured results for the gain and input match are shown in Figs. 12 and 13.

After the analog beamformer, the RF signal must be downconverted to a baseband frequency on the order of 50 MHz for sampling. A prototype downconverter has been fabricated and tested (Fig. 11).

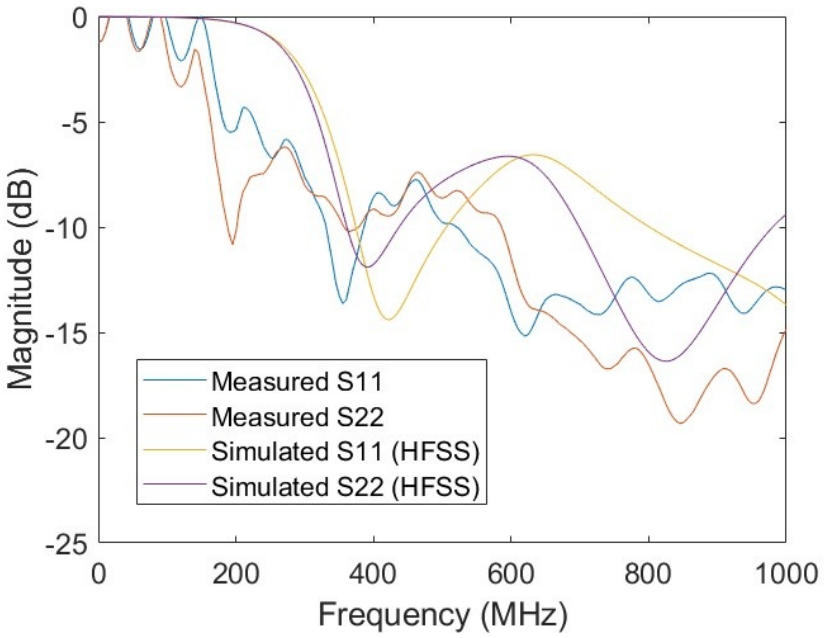

Figure 10. Dual-polarized Vivaldi element prototype return loss.

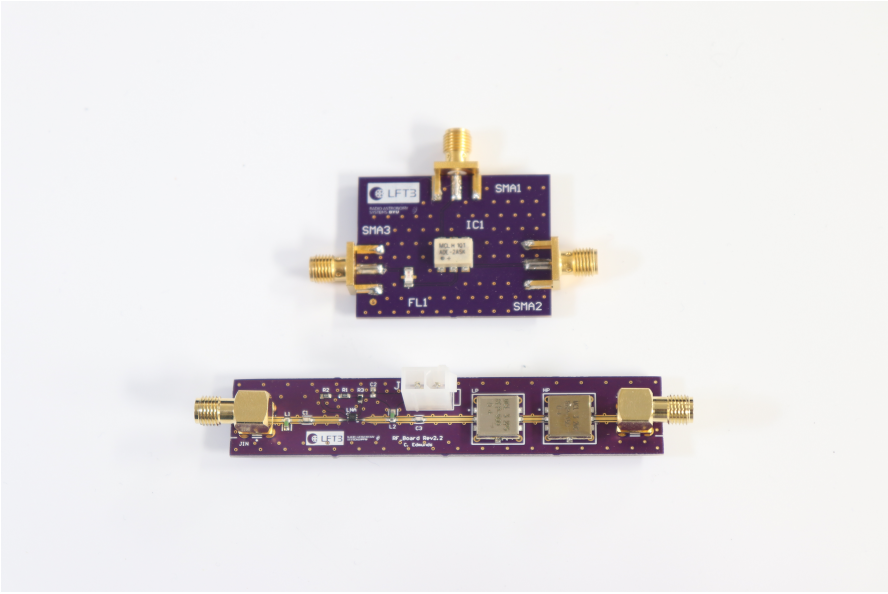

Figure 11. Fabricated LNA (bottom) and downconverter (top).

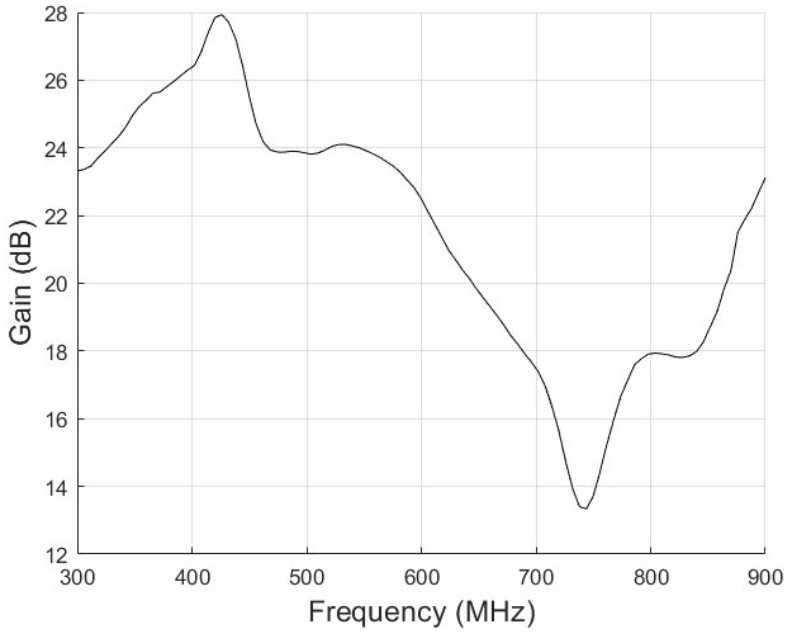

Figure 12. Measured LNA gain.

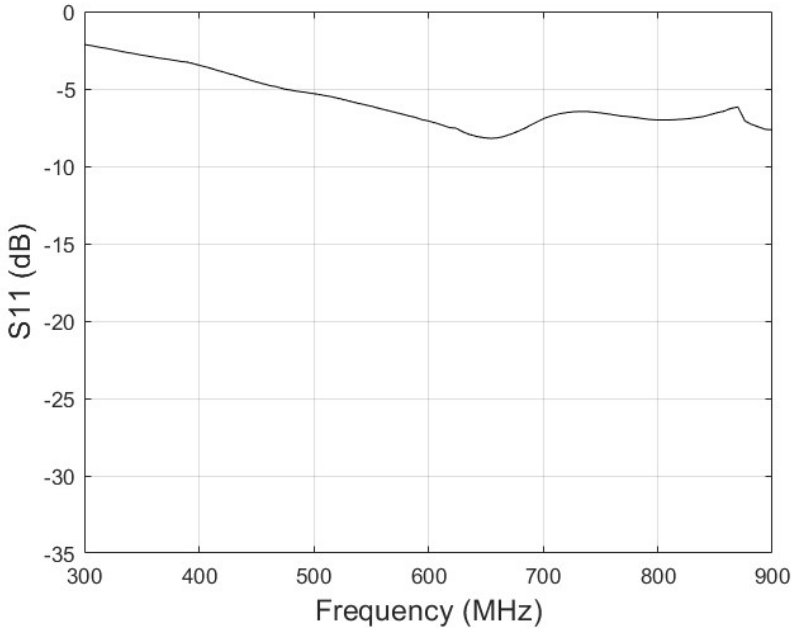

Figure 13. Measured LNA input port reflection coefficient.

2.4. *UHF-Lo Wideband Analog Beamformer*

Designing the LFT3 beamforming network presented a challenge because of the desired wide operating band to form multiple beams with stable steering directions over the 300–900 MHz UHF-Lo operating frequency range. Common analog beamformers such as the Butler matrix (6) have limited bandwidth. To achieve wideband operation, a true time delay (TTD) variant known as a Blass matrix was used.

2.4.1. *Blass Matrix Beamformers*

The Blass matrix is an M-antenna input $\times$ N-beam serial-fed network of couplers and time delay lines (7; 3). At each node in the matrix, a four port network is used to couple signals to beam output ports and to additional beamformer layers in the matrix. Antenna inputs along one edge of the matrix feed a row of directional couplers which are daisy-chained to produce the first beam. Additional rows of couplers can be added to produce an arbitrary number of beams. The delay for each input is caused by cumulative vertical delays and geometric series horizontal delays. Unused ports at the edges of the matrix are terminated with matched loads. The resistive loads dissipate power and introduce loss but avoid reflections of the signal from the edges of the network.

While the delay lines used in the Blass matrix are inherently wideband, the couplers at matrix nodes may include tuned components such as quarter wave lengths of transmission line which introduce unwanted phase delays in the signal paths and can limit the achievable bandwidth. Each coupler adds a frequency-dependent insertion phase that can only be compensated for in adjusting time delays at a single frequency. Across a wide frequency band these phase delays deviate from ideal time delays and lead to beam squint at band edges (8). With suitable wideband couplers at the matrix nodes, Blass matrix designs based on true time delays can achieve up to a 6:1 bandwidth (9).

2.4.2. *Modified Blass Matrix Beamformer*

To ease the difficulty of achieving wideband performance for the Blass matrix and improve the reliability of the beamformer, we have developed a modified Blass matrix beamformer design (Fig. 14) that replaces the four-port couplers with three-port couplers and adds an additional layer of combiners for each beam. In the modified design, signals that are combined for each beam do not propagate through daisy-chained couplers. This approach simplifies the relationship between the line lengths in the network and the time delays needed to form the desired beams. The modified design also reduces multipath through the beamforming network that can occur with the traditional Blass matrix.

The modified Blass matrix requires a multilayer PCB design and an additional combiner for each beam. The LFT3 modified Blass matrix performs beam summations in the combiner, which changes the structure such that each row is parallel-fed rather than serial-fed. For each antenna input, with the modified design the couplers are in parallel rather than in series in the signal paths and the insertion phases introduced by the couplers do not introduce beam errors. Another advantage of the modified Blass matrix is that it eliminates the need for terminating loads on the matrix rows.

To reduce the physical size of the beamformer, the Blass matrix uses a dielectric substrate, and the time delays are implemented as meander lines distributed across the Blass matrix PCB. Beamformers such as the Butler matrix rely on phase shifting elements, which leads to deviation of the beam's pointing angle as the operating frequency changes or beam squint. To reduce beam squint our design relies on a true-time-delay (TTD) network. The time delay needed to steer a beam for a uniform linear array by an angle θ is $\tau = (d \sin\theta)/c$ where d is the element spacing and c is the speed of light. Steering to 45° at 300 MHz ($d \simeq 0.5$ m) requires $\tau \simeq 1.18$ ns, corresponding to about 0.18 m of microstrip or coaxial line assuming

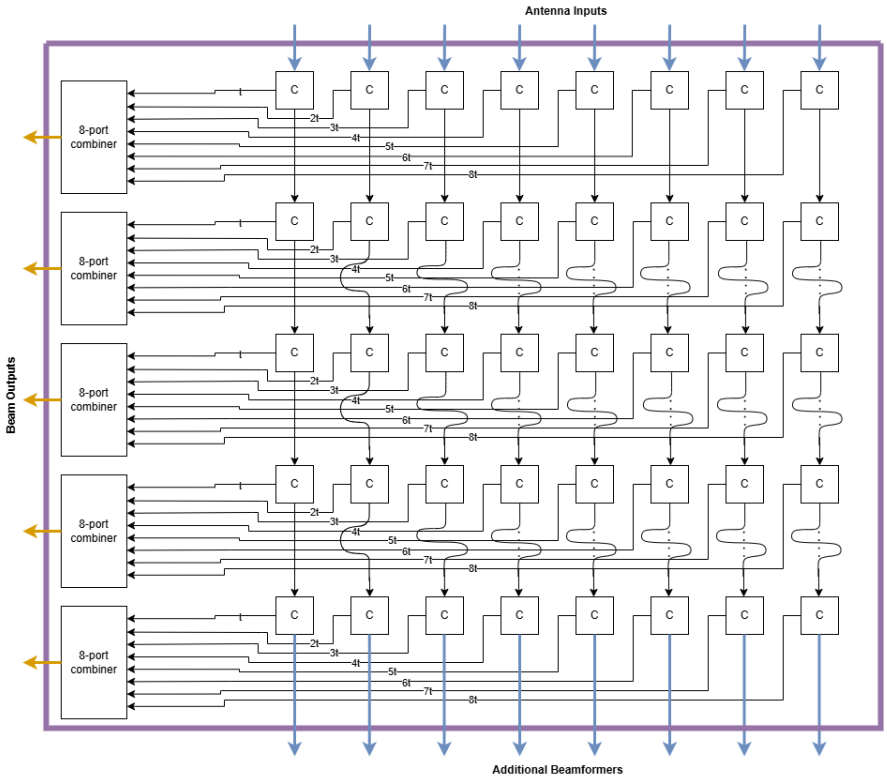

Figure 14. Modified Blass matrix with three-port couplers and combiners for each beam output. At the top are antenna inputs. Beam outputs are on the left. Time delays in the vertical signal paths increase linearly to from left to right. The ports on the bottom of the Blass matrix can be used to cascade multiple Blass matrix boards to produce a larger beamformer, as will be used for LFT3.

an effective permittivity $\varepsilon_r = 4$. Implementing a tree or corporate combining network with such long delay lines would produce a bulky assembly and large insertion loss. Higher dielectric materials are being investigated, which would allow for more miniaturization.

2.4.3. *LFT3 UHF-Lo Prototype Beamformer Fabrication*

The initial LFT3-Lo prototype design had 8 antenna inputs and 5 beam outputs, representing a quarter of the full beamformer for UHF-Lo in one polarization. To test the approach, we fabricated separate Blass matrix rows with 8 inputs and 1 beam output (8×1) before fabricating the 8×5 Blass matrix board. To improve isolation between traces on the top and bottom layers, we chose to use four-layer boards. The substrate material used by the fabricator (OSHPark, Inc.) was Isola FR408HR with dielectric constant 3.7.

Each of the 8×1 prototype boards contains one row of the Blass matrix with 8 antenna inputs. Multiple boards are chained together to produce additional beams. Based on the calculated delays, our Blass matrix design has two unique rows requiring two PCB designs. The first row has geometrically increasing horizontal delays but no vertical delays. The second row has the same horizontal delays but requires meanders for the vertical delays.

The measured isolation between traces on these PCBs was 45 dB in the worst case. The insertion loss from antenna inputs (top) to coupler outputs (bottom) is less than 1 dB (Figures 16 and 18). The insertion loss from antenna inputs to combiner output is roughly 34 dB across the band for both boards (Figures 15 and 17).

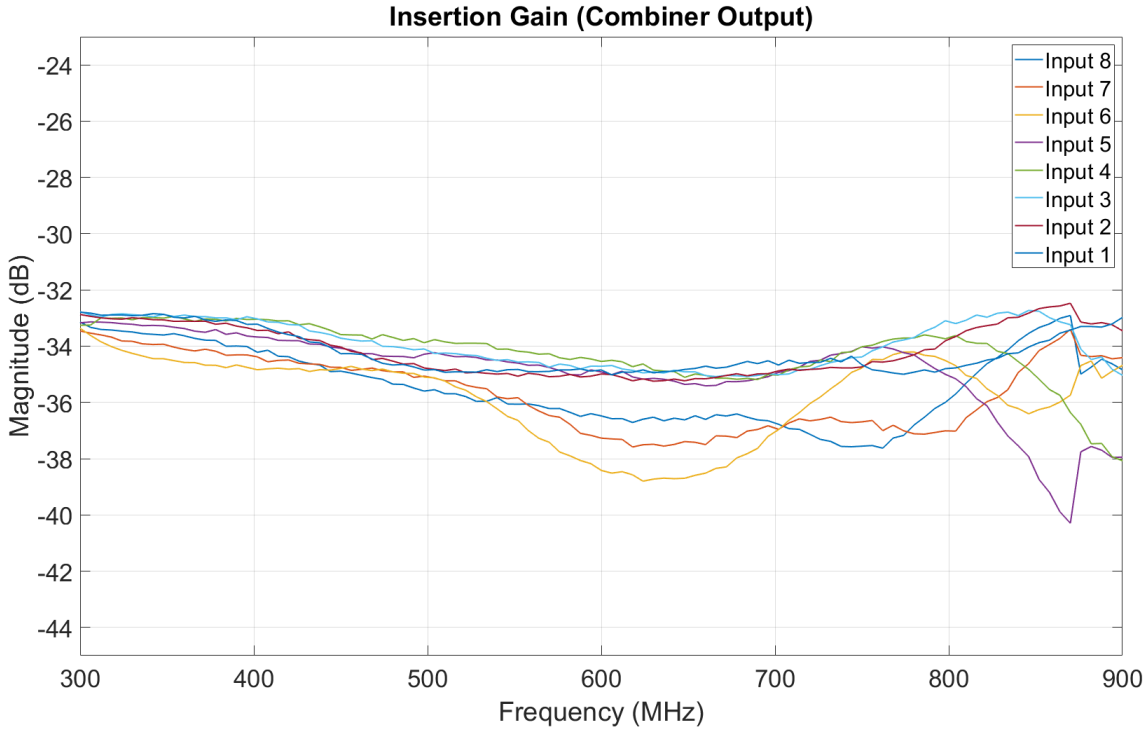

Figure 15. S21 magnitude measured from antenna inputs to the combiner output for the first Blass matrix row PCB.

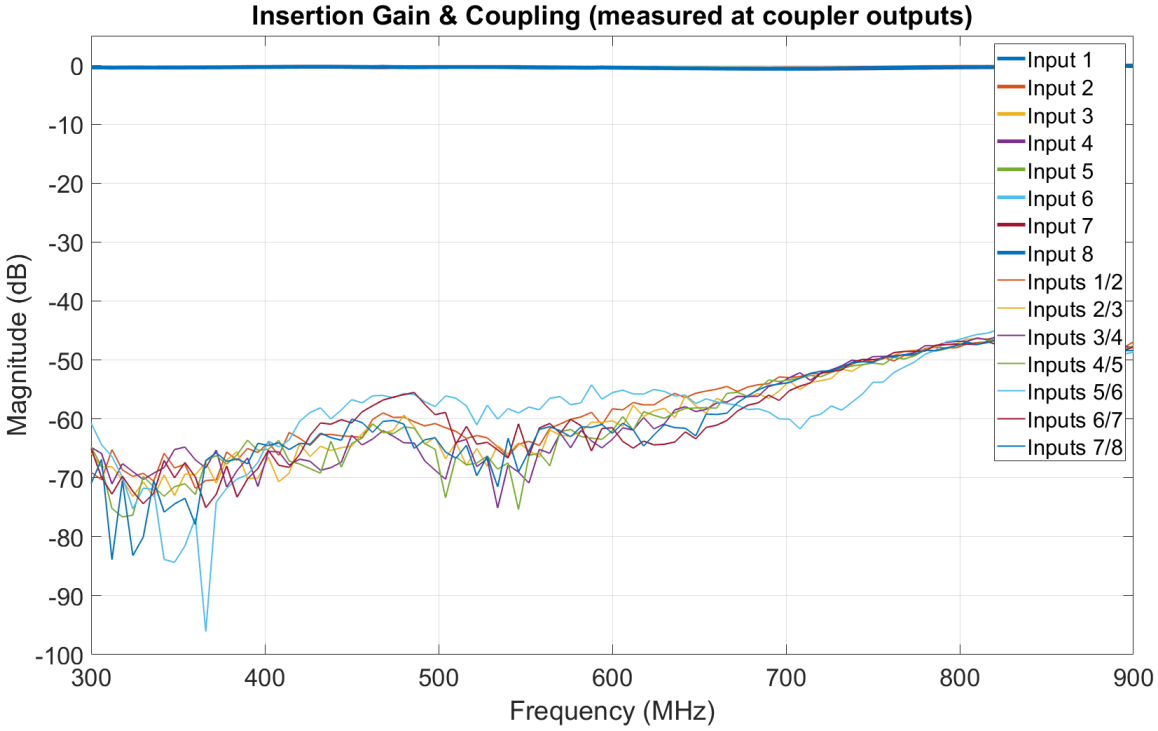

Figure 16. S21 magnitude measured from antenna inputs to coupler outputs of the first row PCB.

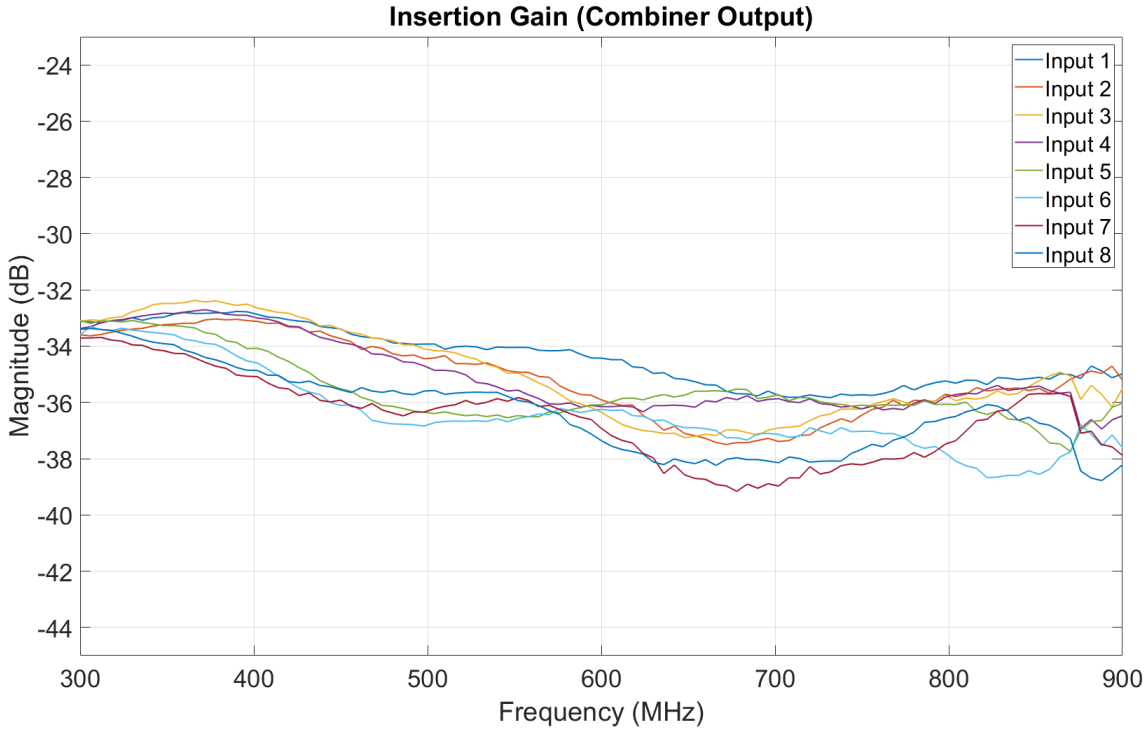

Figure 17. S21 magnitude measured from antenna inputs to combiner output of the second Blass matrix row PCB.

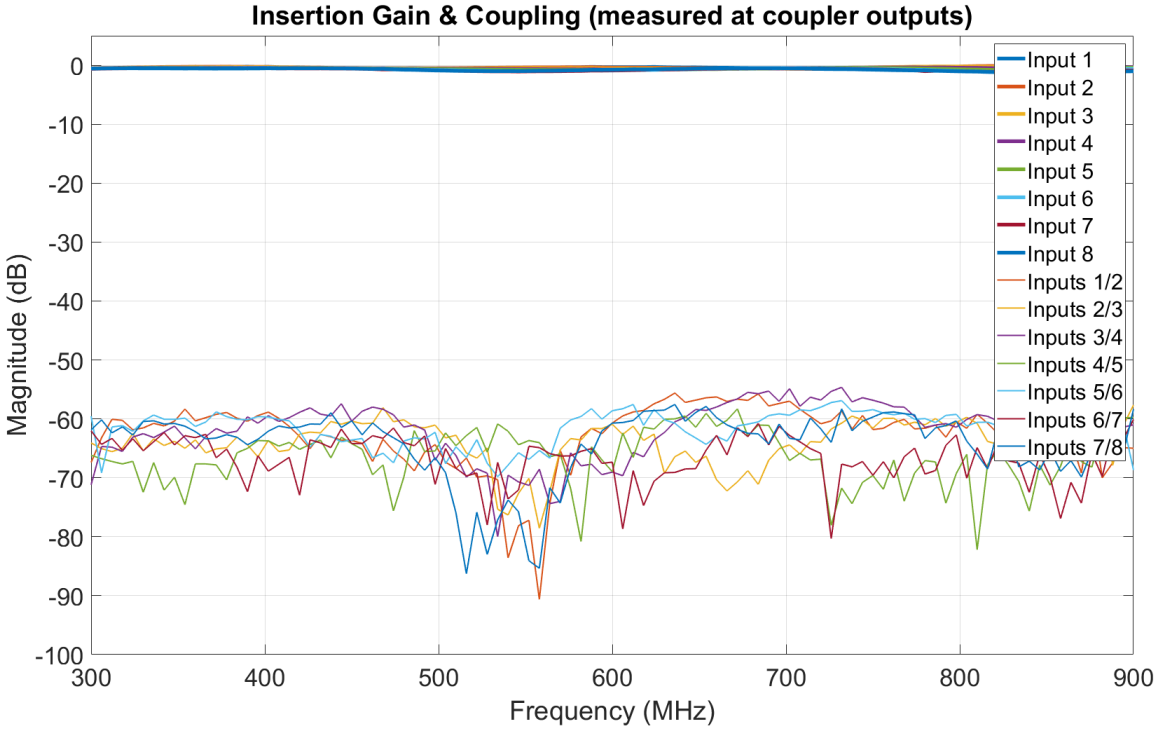

Figure 18. S21 magnitude measured from antenna inputs to coupler outputs of the second row PCB.

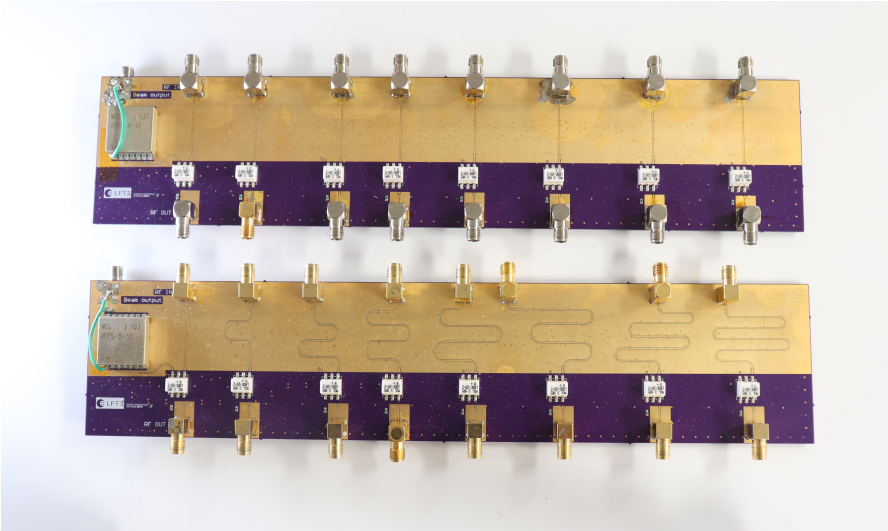

Figure 19. Two single beam and 8 input Blass matrix row PCBs with different time delay meander line lengths in the second PCB.

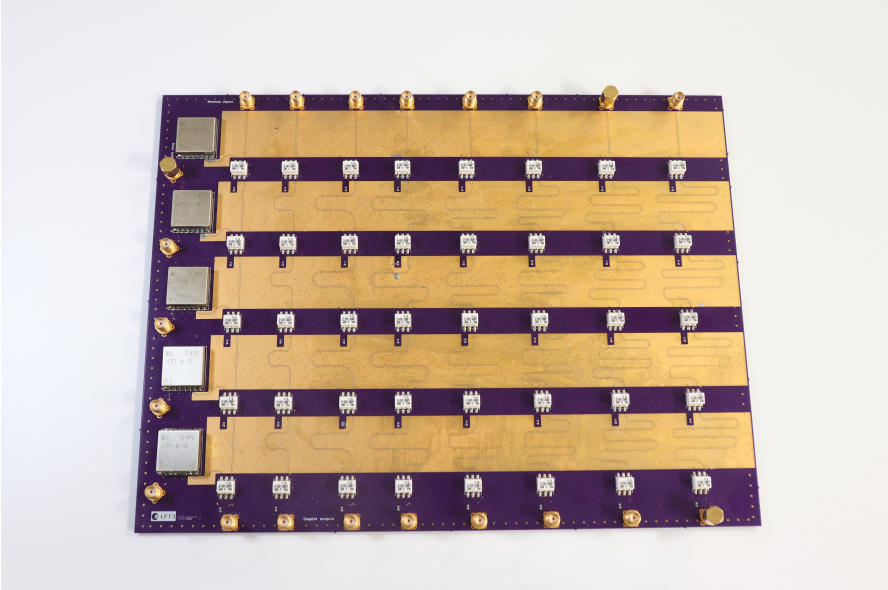

Figure 20. Fabridated PCB with 8 input 5 beam modified Blass matrix, or one quarter of a full single polarization beamformer for the LFT3 UHF-Lo receiver.

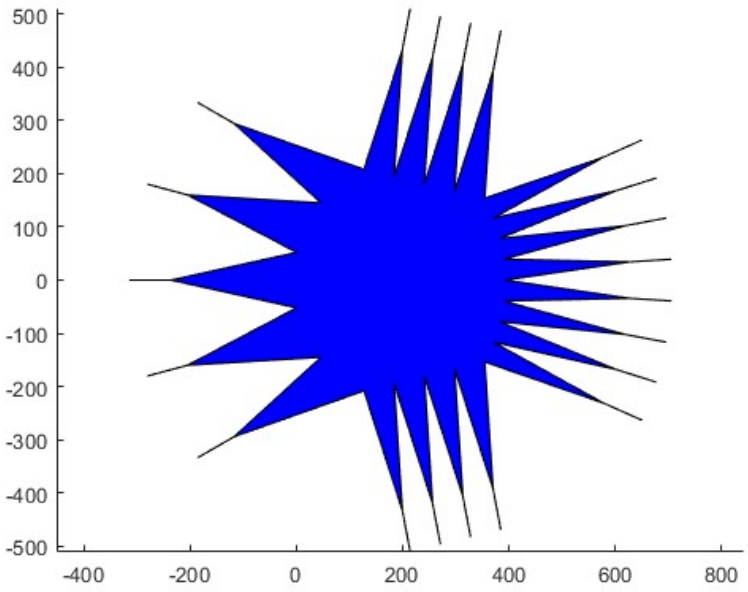

Figure 21. 900–2700 MHz Rotman lens design for ε_r = 4.5.

2.5. *UHF-Hi Rotman Lens Beamformer*

For the UHF-Hi array, shorter wavelengths across the operating bandwidth allow for a wider range of design possibilities for the beamformer while maintaining acceptable physical dimensions. One approach to a compact beamformer for phased arrays is a Rotman lens. A Rotman lens is a true-time-delay approach for wideband antenna arrays to achieve low-cost beamforming with a corporate structure.

A prototype design for the UHF-Hi Rotman lens was developed using the approach of Ref. (10). The design center frequency was 1.8 Ghz. The number of antenna input ports was eight and the number of beam output ports is five. The beam steering angle increment was 30°. Once the number of antenna input and beam ports is fixed, the Rotman lens design is controlled by a focal ratio and an expansion factor. The focal ratio β controls how far the off-axis focal points (edge beams) are from the lens compared to the on-axis focal point (boresight beam). For $\beta < 1$, the lens becomes smaller and more compact but can also exhibit increased beamformer phase error. A focal ratio of $\beta = 0.9$ was selected to make the design reasonably compact without causing significant phase errors. The expansion factor γ controls the relationship between the array port locations and the beam port locations. Ref. (10) used $\gamma = 1$ for a linear mapping between beam ports and array ports and symmetric beam spacing and the simplest and most stable design.

A primary design variable explored during development of the Rotman lens was the substrate permittivity. The initial design assumed a high-permittivity substrate of ε_r = 9.8. The dielectric constant was later adjusted to ε_r = 4.5 to match readily available substrate materials. Reducing the dielectric permittivity from 9.8 to 4.5 significantly lowered the material cost for the fabricated prototype at the expense of an increase in the physical footprint (from 700 mm × 700 mm to 1020 mm × 1020 mm).

The Rotman lens design is shown in Figs. 21 and 22. The side ports are terminated with a matched load. Simulated results for the S-parameters of the structure are shown in Figs. 23 and 24. Insertion loss between the antenna inputs and the beam outputs is on the order of 15 dB.

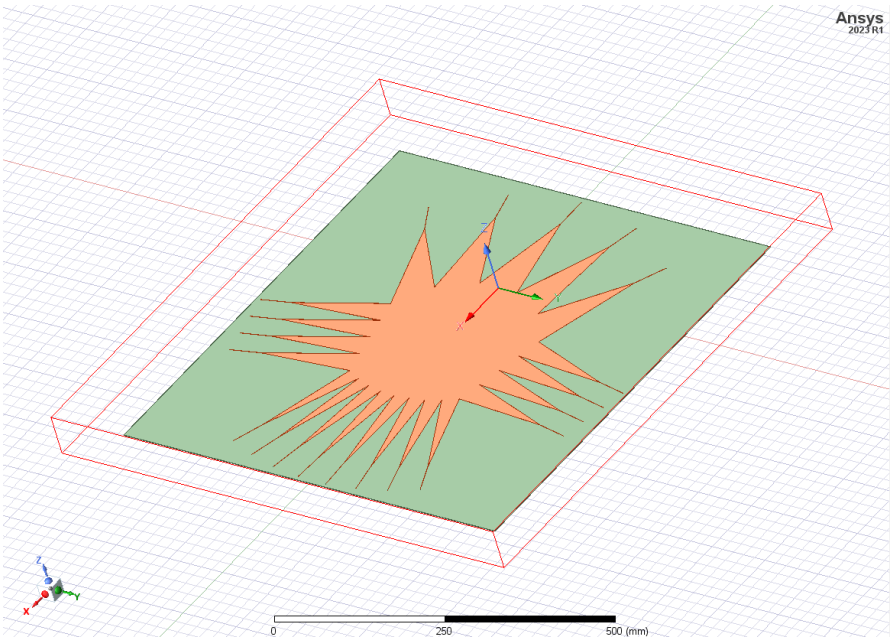

Figure 22. Rendering of the UHF-Hi Rotman lens design.

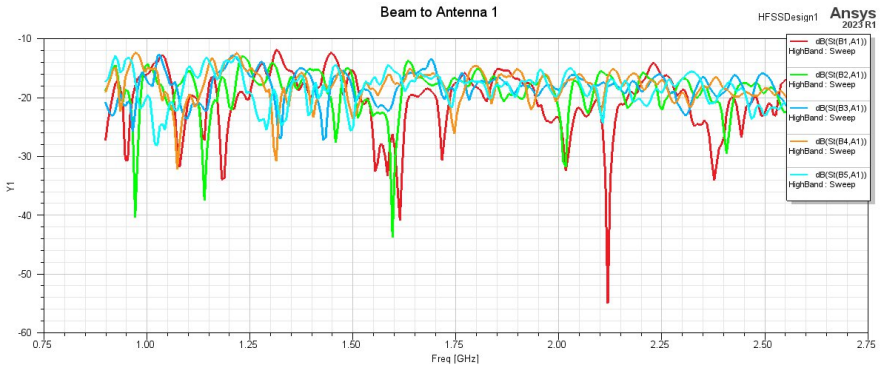

Figure 23. Simulated results for S-parameters at antenna input 1.

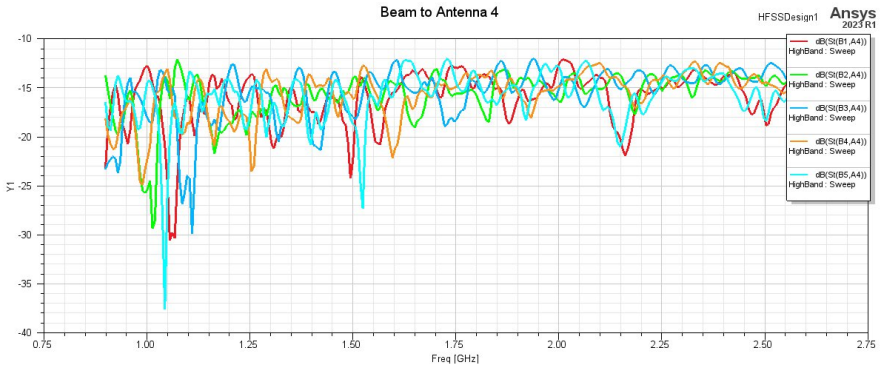

Figure 24. Simulated results for S-parameters for antenna input 4.

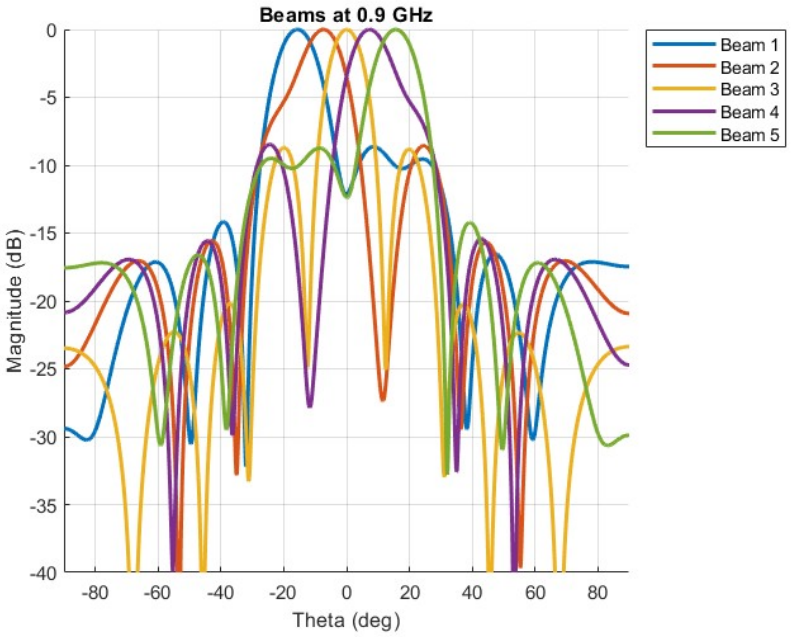

Figure 25. Beam patterns at 0.9 GHz computed using simulated S-parameters for the Rotman lens design.

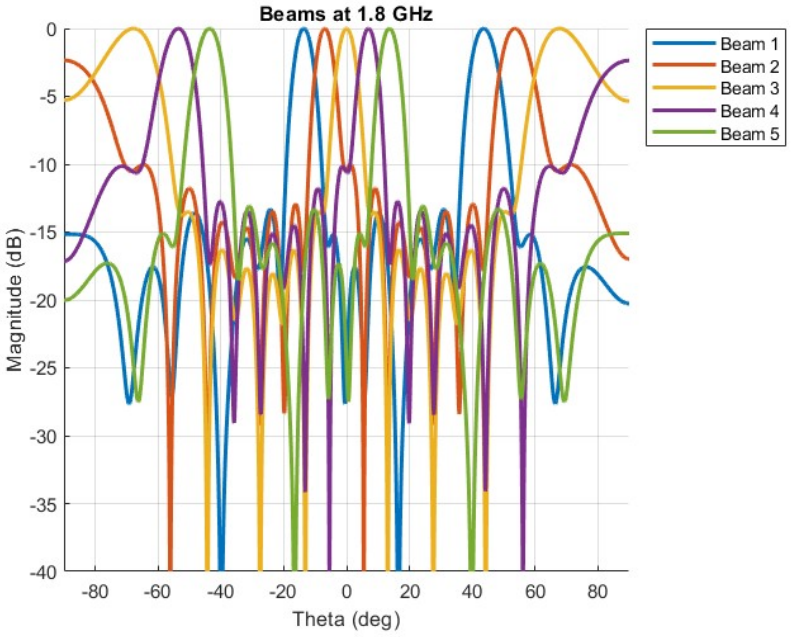

Figure 26. Simulated beam patterns with the Rotman lens at 1.8 GHz.

Beam patterns computed using simulated S-parameters at the band edges and center are shown in Figures 25, 26, and 27. Fabrication and experimental validation of the finalized lens design are currently underway. Additionally, higher dielectric constant substrates are being investigated for further miniaturization of the Rotman lens.

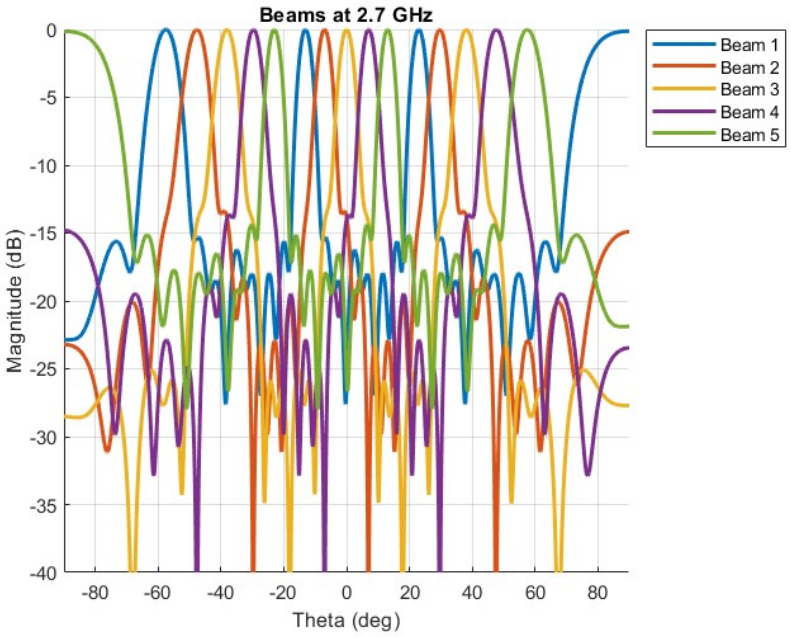

Figure 27. Simulated beam patterns with the Rotman lens at 2.7 GHz.

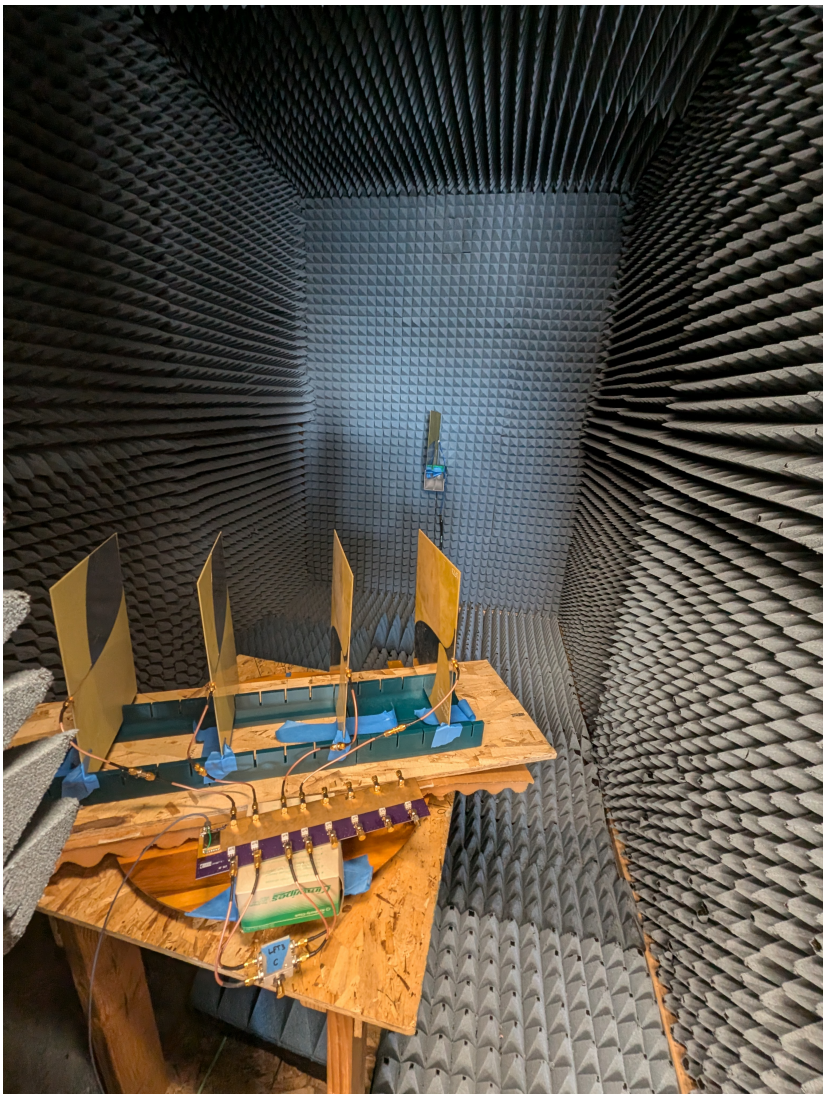

Figure 28. Prototype array with 4 receive antennas.

3. BEAMFORMER VALIDATION AND MEASUREMENT

A fabricated UHF-Lo modified Blass matrix beamformer prototype board was tested by measuring the insertion gain and phase (S21) from each antenna input to the coupled output port of the couplers that feeds a row beam combiner. The S21 magnitude reflects amplitude variations between channels which could distort the beam pattern. The unwrapped S21 phase from antenna input to coupler output indicates the delay that the BFN applies to the antenna signal before the summation. The S21 parameters for each line are equivalent to the beamformer weights applied by the matrix. These weights were used in post processing to create beam patterns by digitally sweeping the angle of a simulated input signal. These curves are labelled as "Measured on NanoVNA" in Figures 29, 30, and 31.

The beam pattern achieved by the Blass matrix board was also verified using over-the-air tests with an antenna array. Four Vivaldi antennas were connected to the first four inputs of the first row of the Blass matrix. The beam output was connected to a spectrum analyzer. A tone was transmitted from a transmit

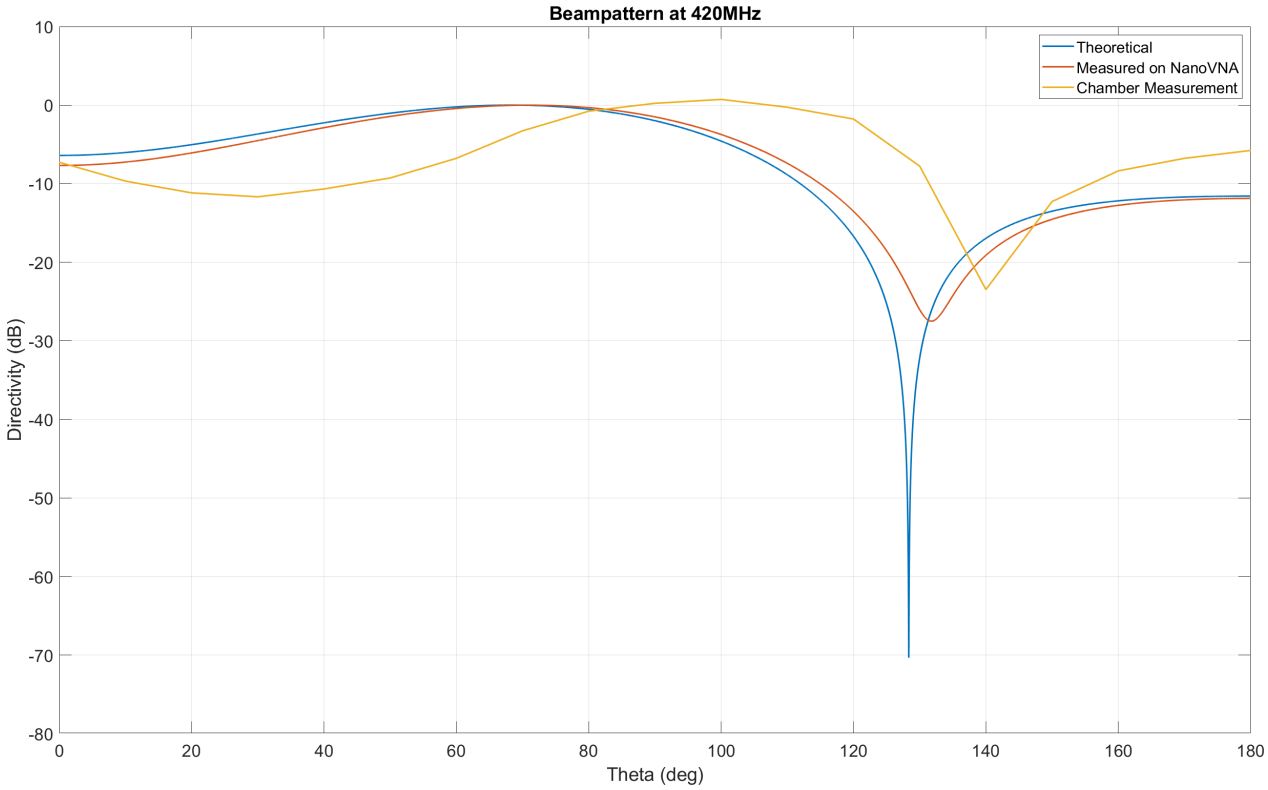

Figure 29. Theoretical beam pattern compared to beam patterns computed from S-parameter measurements of the beamformer board insertion phase ("Measured on NanoVNA") and patterns measured in an antenna range at 420 MHz for the first 4 ports of the 8-port board with 18 cm spacing between elements ("Chamber Measurements").

antenna located opposite the Vivaldi array, and the tone power was recorded as the array was rotated in 10 degree increments. The beam pattern was measured with the transmit and receive in several configurations.

The receive antennas were originally spaced 18 cm apart to mimic the row spacing in the final array. The antenna chamber has the transmitter attached to the far wall of the chamber. The receiver is placed on a rotating turntable on a plywood stool with 10 degree increments marked in pen (Figure 28). We then measured the beam pattern for the first row by connecting a spectrum analyzer (TinySA) to the on-board 8:1 combiner. Figures 29, 30, and 31 shows the measured beam pattern at 420 MHz. The nulls are visible but the angles are slightly off due to misalignment, coupling, and scattering effects.

The second beam pattern was more challenging to measure because the beam is steered further off bore-sight, where coupling and other electromagnetic effects become more prominent. To reduce the effect of coupling we used a 31.5 cm spacing and reduced the array to 3 receive antennas (Figure 32). After making these changes we were able to measure the beam pattern in Figure 33.

To facilitate rapid testing of analog beamformers, we have developed an FPGA-based array emulator. The array emulator was implemented on a Xilinx RFSoC ZCU208 FPGA board and produces multiple digitally synthesized sinusoidal waveforms with variable phase delays. The RFSoC board digital to analog converters (DACs) generate phase delayed sinusoids which are fed to the BFN. The output of the beamformer is routed to analog to digital converters (ADCs) on the same board and a spectrometer to record the beam output power. Sweeping the phase delays between the sinusoids on each port produces a beampattern over angle. These digitally produced beampatterns allowed us to verify the operation of the second beam at the lower end of the band (Figure 34).

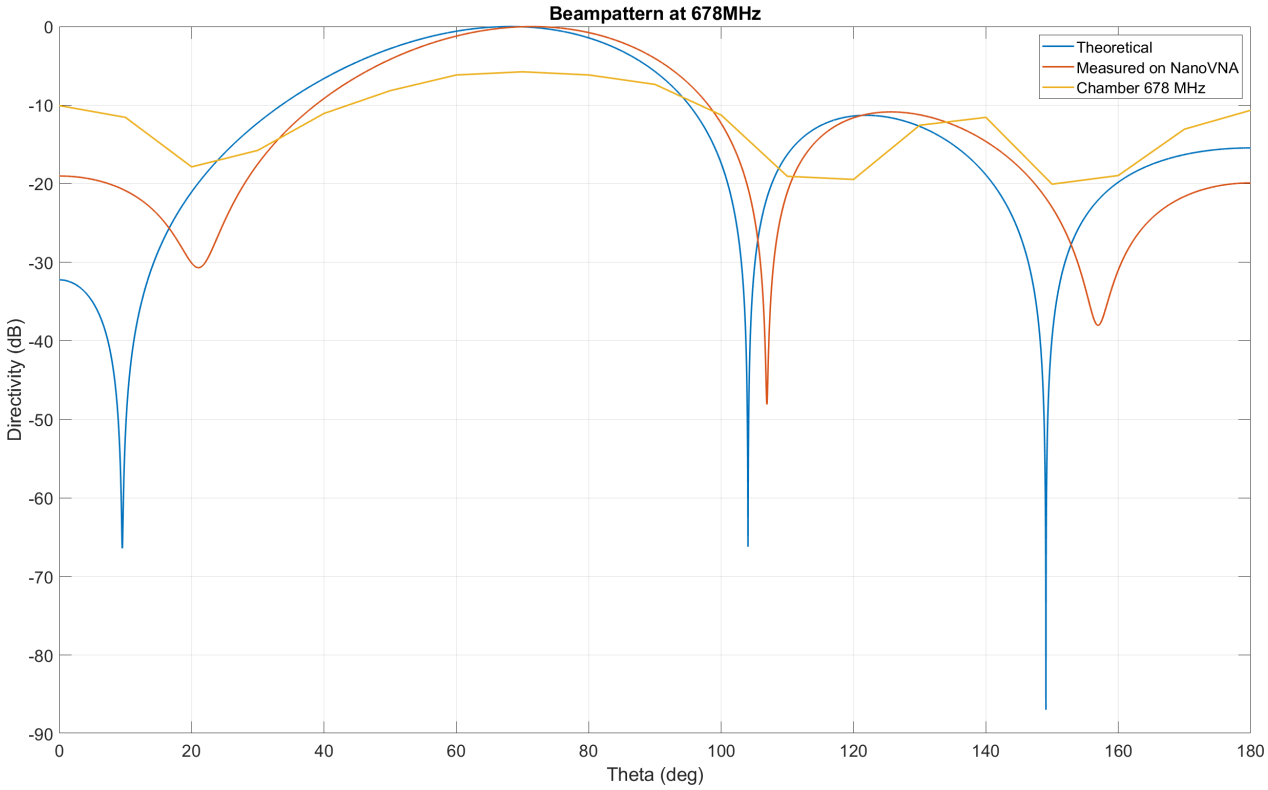

Figure 30. Theoretical and measured beam patterns at 678 MHz for the first 4 ports of the first 8-port Blass matrix row PCB with 18 cm spacing between antenna elements.

To take the first steps toward full system integration, additional tests were done with the RF chain components described in Sec. 2.3 connected to the Blass matrix beamformer board as shown in Fig. 35. The first column of the matrix was used in testing the full receiver chain with a single Blass matrix board input. A 600 MHz tone at -10 dBm was input to the LNA from a signal generator, propagated to the Blass matrix combiners, and mixed down to 400 MHz. This 400 MHz tone is visible on the spectrometer output with an output power of -26.7 dBm (Figure 36).

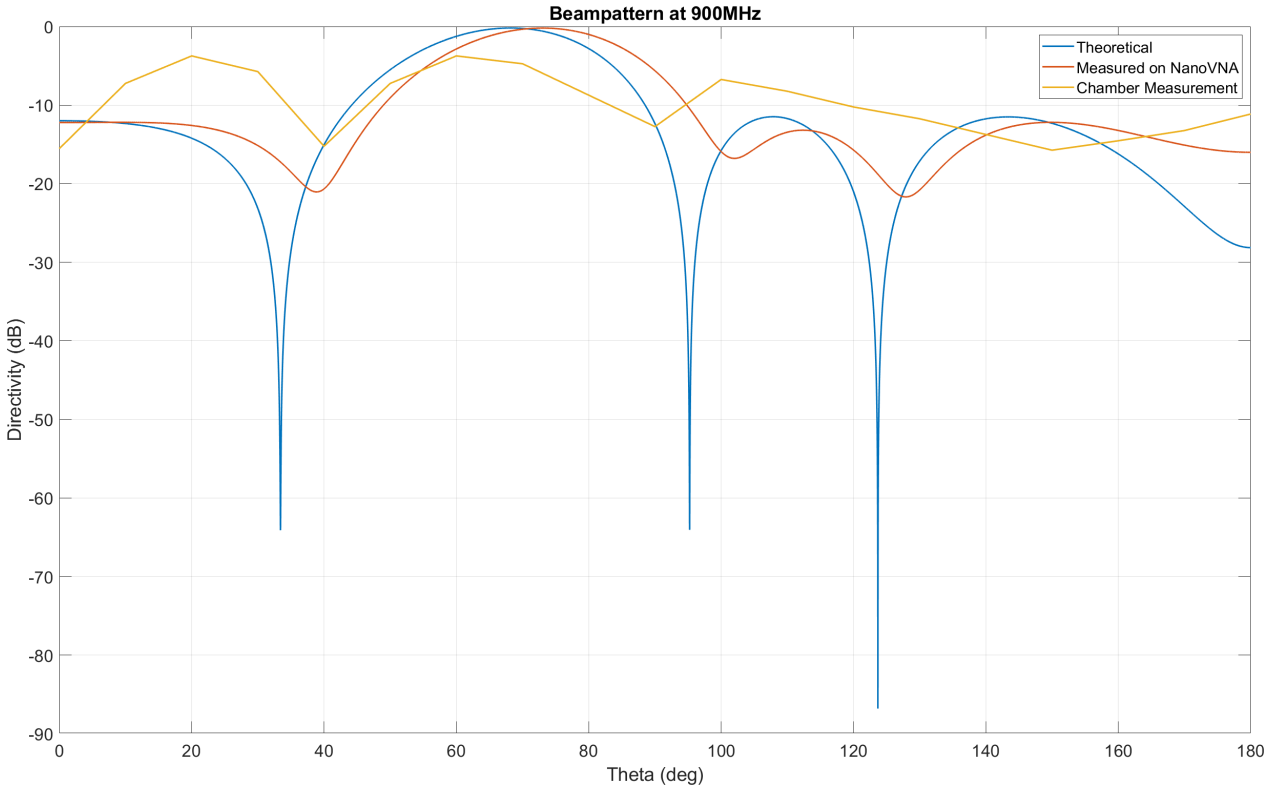

Figure 31. Theoretical and measured beam patterns for the first Blass matrix row at at 900 MHz.

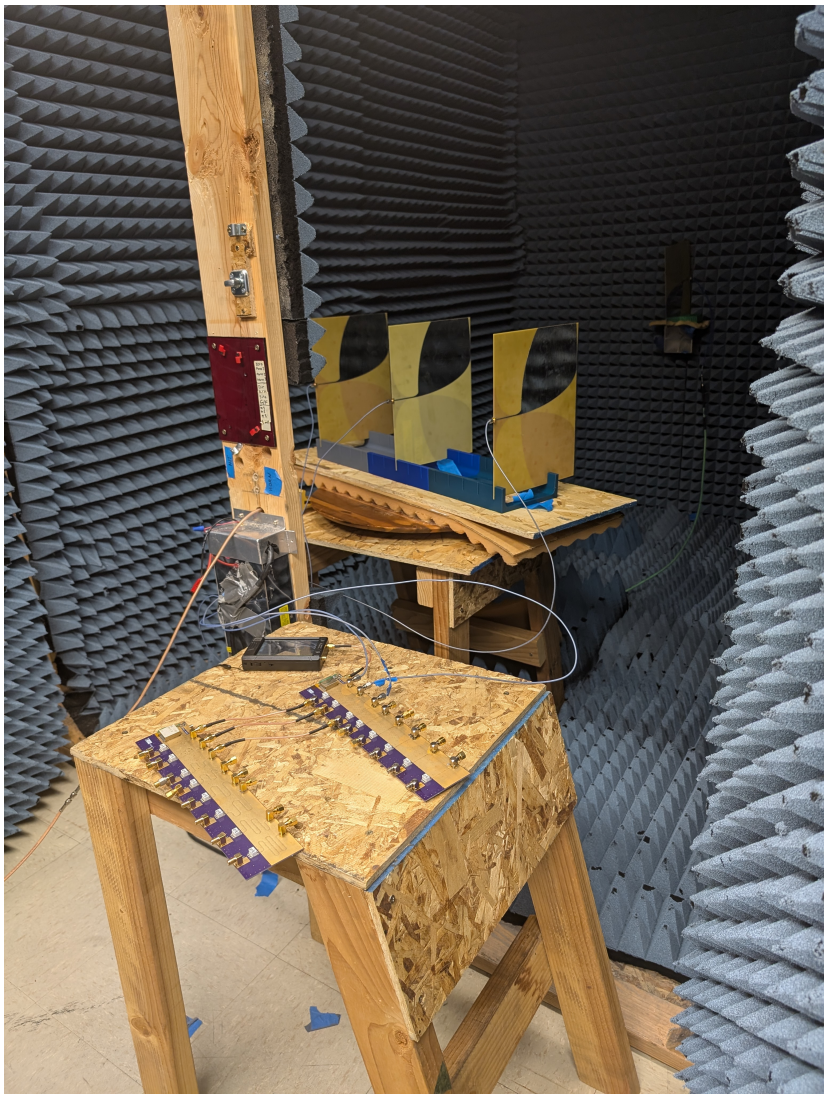

Figure 32. Prototype array with three receive antennas and off-board 4:1 combiner to produce a boresight beam

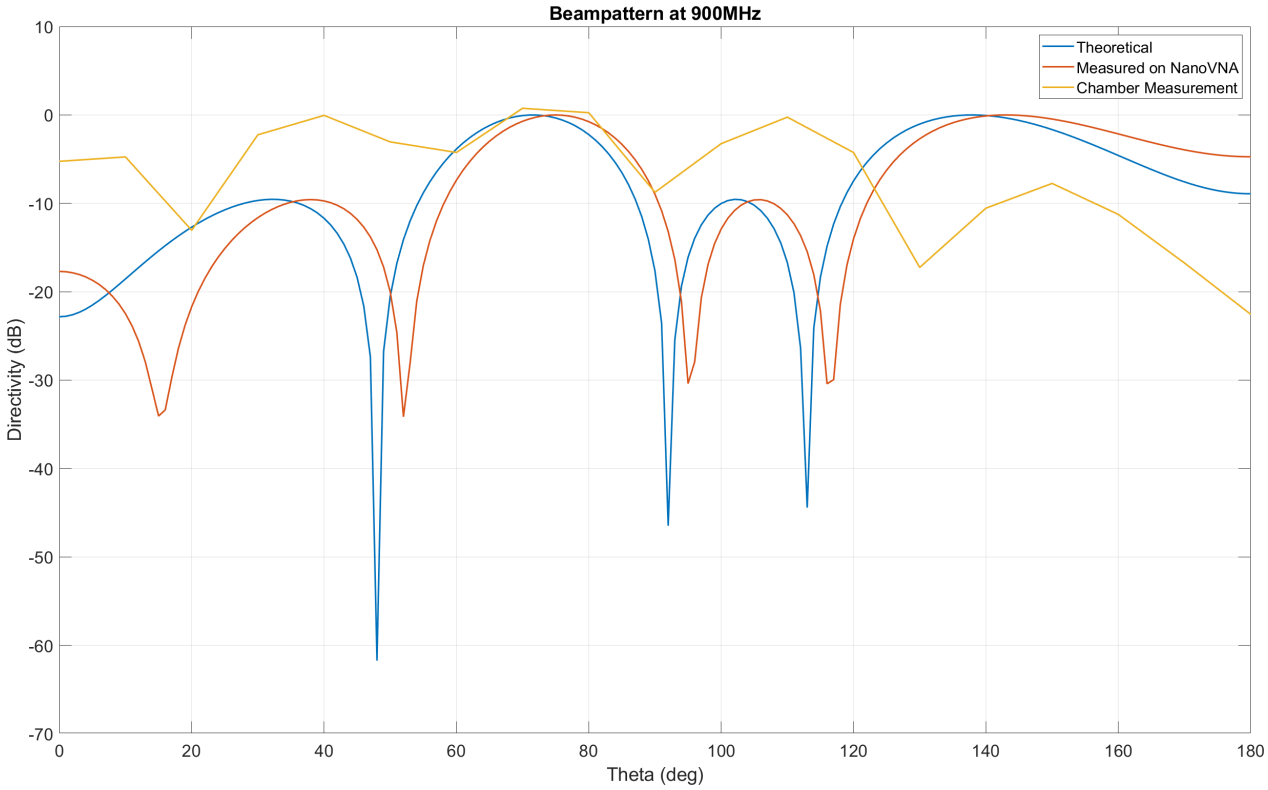

Figure 33. Theoretical and measured beam patterns at 900 MHz for the first three ports of the second 8-port Blass matrix row PCB with 31.5 cm spacing between antenna elements.

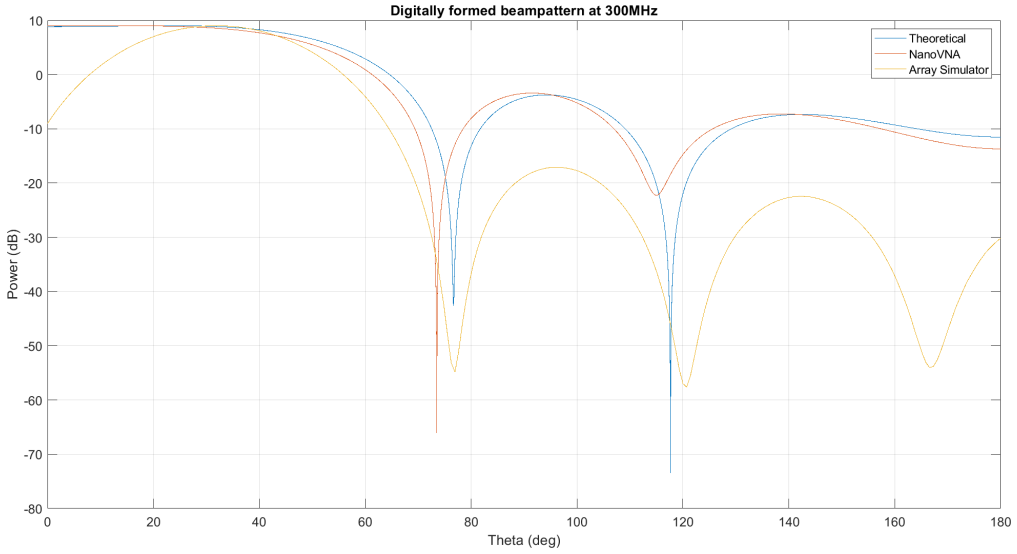

Figure 34. Theoretical and measured beam patterns at 300 MHz for all input ports of the second 8-port Blass matrix row PCB with 18 cm spacing between elements including results from an FPGA-based array emulator.

Figure 35. Receiver chain setup. A signal generator (left) feeds an LNA that drives the first column of the Blass matrix board. The first four beam outputs are downconverted and sampled using a Xilinx ZCU208 RFSoC board.

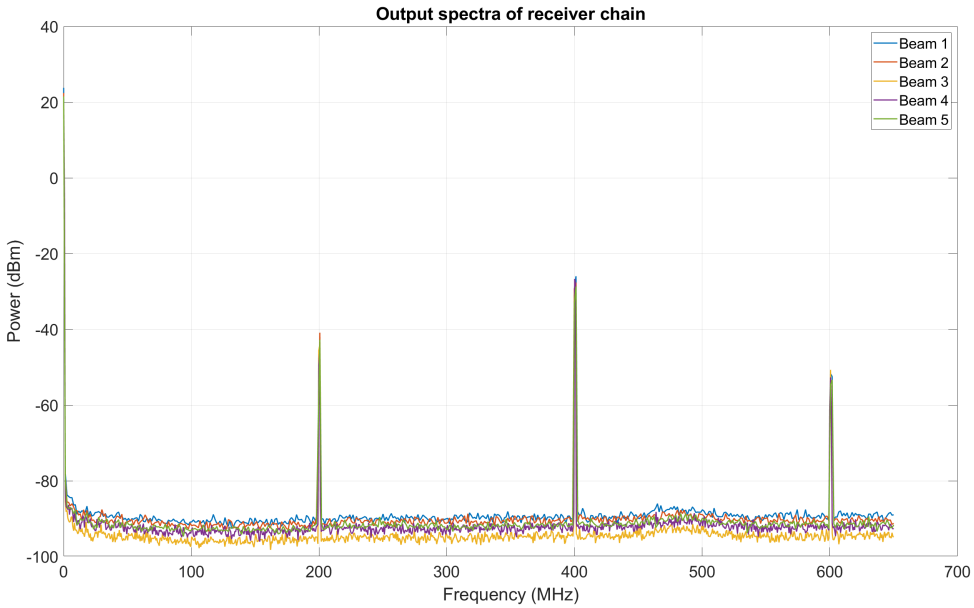

Figure 36. Beam outputs of receiver chain measured on TinySA. A -10 dBm tone was amplified by 35 dB, passed through the first antenna input, and the beam outputs were mixed down from 600 MHz to 400 MHz (LO set at 200 MHz).

4. CONCLUSION AND FUTURE WORK

The goal of this work was to develop design approaches for each major element of the LFT3 UHF array receivers, including antenna elements, array geometry, beamformers, and RF signal handling. For the UHF-Lo array, the Blass matrix approach to a low-power wideband analog beamformer has been vetted through prototype testing and appears to be an innovative and effective solution that meets design requirements for the receiver. To achieve wider bandwidth than traditional Blass or Butler matrix beamformers, we have developed a modified Blass matrix that eliminates phase shifts in the couplers at nodes in the beamforming network. We are currently fabricating a full size beamformer using four PCBs and connectorized interconnects to daisy-chain the boards and provide 16 antenna port inputs and 10 beam outputs. Testing of a Rotman lens for the UHF-Hi beamformer is underway.

REFERENCES

[1]D. R. DeBoer, C. K. Ashe, O. A. Johnson, E. F. Keane, A. C. Lesh, E. J. Marshall, S. Prabu, K. L. Reenock, A. Slosar, C. D. Tremblay, J. D. Turner, K. F. Warnick, A. P. V. Siemion, J. Drew, and S. P. Worden, "LFT3 memo 1: Lunar farside technosignature and transient telescope (LFT3)," https://lft3.space/memos/memo1.pdf, Dec. 2025.

[2]N. Fagnoni, E. de Lera Acedo, N. Drought, D. R. DeBoer, D. Riley, N. Razavi-Ghods, S. Carey, and A. R. Parsons, "Design of the new wideband Vivaldi feed for the HERA radio-telescope phase II," *IEEE Transactions on Antennas and Propagation*, vol. 69, no. 12, pp. 8143–8157, 2021.

[3]S. Mosca, F. Bilotti, A. Toscano, and L. Vegni, "A novel design method for Blass matrix beam-forming networks," *IEEE Transactions on Antennas and Propagation*, vol. 50, no. 2, pp. 225–232, 2002.

[4]D. I. Lialios, C. L. Zekios, and S. V. Georgakopoulos, "A new class of full-dimensional planar true-time-delay beamforming networks," *IEEE Transactions on Antennas and Propagation*, vol. 72, no. 3, pp. 2337–2346, 2024.

[5]S. Prabu, D. R. DeBoer, C. K. Ashe, O. A. Johnson, E. F. Keane, C. D. Tremblay, and K. F. Warnick, "LFT3 memo 2: LFT3 science operations — initial design framework," https://lft3.space/memos/memo2.pdf, Dec. 2025.

[6]M. Bona, L. Manholm, J. Starski, and B. Svensson, "Low-loss compact Butler matrix for a microstrip antenna," *IEEE Transactions on Microwave Theory and Techniques*, vol. 50, no. 9, pp. 2069–2075, 2002.

[7]J. Blass, "Multidirectional antenna - a new approach to stacked beams," in *1958 IRE International Convention Record*, vol. 8, 1960, pp. 48–50.

[8]Y. J. Guo, M. Ansari, and N. J. G. Fonseca, "Circuit type multiple beamforming networks for antenna arrays in 5G and 6G terrestrial and non-terrestrial networks," *IEEE Journal of Microwaves*, vol. 1, no. 3, pp. 704–722, 2021.

[9]D. I. Lialios, C. L. Zekios, S. V. Georgakopoulos, and G. A. Kyriacou, "A novel rf to millimeter waves frequency translation scheme for ultra-wideband beamformers supporting the sub-6 ghz band," *IEEE Transactions on Antennas and Propagation*, vol. 70, no. 12, pp. 11 718–11 733, 2022.

[10]M. Pokorny. (2019) Rotman lens design with HFSS link. MATLAB Central File Exchange. [Online]. Available: https://www.mathworks.com/matlabcentral/fileexchange/50490-rotman-lens-design-with-hfss-link